Heliyon

*Received:*
12 June 2018
*Revised:*
14 September 2018
*Accepted:*
1 February 2019

Cite as:
Venkata Rao Madduluri, Naresh Kumar Katari, Nagaiah Peddinti, Challa Prathap, David Raju Burri, Seetha Rama Rao Kamaraju, Sreekantha B. Jonnalagadda. Unique Lewis and Bronsted acidic sites texture in the selective production of tetrahydropyran and oxepanefrom1,5-pentanediol and 1,6-hexanediol over sustainable red brick clay catalyst. Heliyon 5 (2019) e01212.
doi: 10.1016/j.heliyon.2019.e01212

# Unique Lewis and Bronsted acidic sites texture in the selective production of tetrahydropyran and oxepanefrom1,5-pentanediol and 1,6-hexanediol over sustainable red brick clay catalyst

**Venkata Rao Madduluri** [a], **Naresh Kumar Katari** [b,c,*], **Nagaiah Peddinti** [a], **Challa Prathap** [a], **David Raju Burri** [a], **Seetha Rama Rao Kamaraju** [a], **Sreekantha B. Jonnalagadda** [c,*]

[a] *Inorganic and Physical Chemistry Division, CSIR-Indian Institute of Chemical Technology, Hyderabad 500007, India*

[b] *Department of Chemistry, GITAM School of Technology, GITAM Deemed to be University, HTP Campus, Rudraram, Medak, Telangana 502 329, India*

[c] *School of Chemistry & Physics, University of KwaZulu-Natal, P Bag X 54001, Durban 4000, South Africa*

[*] Corresponding author.

E-mail address: Jonnalagaddas@ukzn.ac.za (S.B. Jonnalagadda).

## Abstract

Activated red brick (ARB) clay material proved superb catalyst for selective conversion of 1,5-pentanediol (1,5-PDO) to tetrahydropyran (THP) and 1,6-hexanediol (1,6-HDO) to oxepane (OP) *via* dehydration under vapor phase conditions in a continuous flow reactor. As per scanning electron microscopy (SEM), SEM-EDX and X-ray fluorescence (XRF) techniques, ARB clay catalyst majorly possessed silica (quartz), and iron oxide (hematite) species, and

https://doi.org/10.1016/j.heliyon.2019.e01212

synergistic texture contributed to the catalytic efficiency for prolonged time-on-stream (TOS). The combination of active Lewis and Bronsted acidic sites with weak to mild acidic nature in the ARB clay obviously facilitates the dehydration reaction with high selectivity, tetrahydropyran (82%) and oxepane (89%). ARB clay displayed superior catalytic properties in the dehydration of alcohols compared with activities of commercial silica and $\alpha$-$Fe_2O_3$ as catalysts. Commercial silica and $\alpha$-$Fe_2O_3$ catalysts possessing the Lewis acidic sites only did not facilitate synchronous dehydration mechanism.

Keywords: Physical chemistry, Materials chemistry, Inorganic chemistry

## 1. Introduction

In recent years, the use of tetrahydropyran (THP) and oxepane (OP) as useful commodities and renewable feedstocks is significantly increased in the chemical industry and for various industrial applications [1, 2]. Hence, there is also growing interest in conversion of 1,5-pentanediol (1,5-PDO) and 1,6-hexanediol (1,6-HDO) alcohols to valuable tetrahydropyran and oxepane products respectively. Tetrahydropyran can be used as both a solvent and an intermediate in the synthesis of organic compounds, such as glutaric acid, 1,5-dichloropentane, heptanediamine, and pimelic acid [1]. Oxepane (OP) is also a valuable intermediate for various medical and biological products. Synthesis of oxepane ring *via* ring formation metathesis [2] and the production of oxepane derivatives by an exo-mode cyclization has been reported using different reagents such as lead tetraacetate, N-(phenylthio)-morpholine, (phenylseleno)phthalimide, and mercuric and palladium salts [3]. The formation of oxepane derivatives by an endo-mode cyclization is also possible using strong acids like telluric derivatives and palladium salts [3]. In broad sense, very few results appeared about conversion to larger ring sizes, that too with low yields. However, the reaction of an unsaturated isoxazoline with iodine was reported to give a 2-(iodomethyl)oxepane in good yields [3].

In conventional methods, various experimental procedures using different catalysts were described for liquid phase dehydration of variety of alcohols [3, 4]. Thereby, different aliphatic ethers were prepared from removal of water from corresponding alcohols. Nevertheless, this was unsuccessful for the preparation of oxacyclanes (larger size cyclic ethers) from different aliphatic alcohols [4]. In recent years, synthesis of aliphatic oxacyclanes has been reported through several organic catalysts such as carbodiimide, dimehylsulfoxide, and sulforane [4]. Primarily to prepare these materials significantly require scarce reagents and oxacyclanes yields were still low [4]. Inoue et al., reported the dehydration of numerous aliphatic alcohols into corresponding oxacyclane products $<$70 % yields *via* distillation method using alumina as catalyst [4]. In conventional alcohols dehydration process, several


https://doi.org/10.1016/j.heliyon.2019.e01212

mineral acids were often used, among those, few catalysts were corrosive and needing neutralizing agents, which lead to environmental pollution [5]. Furthermore, difficulties in separation of used catalyst and low yields of desired products in batch mode limit their application towards large-scale production.

In this perspective, vapor phase is a continuous flow process, which generates value-added products with better yields at atmospheric pressure will be an attractive proposition. For vapor phase reactions, numerous solid oxide catalysts such as, bixbyite $Sc_2$-x$YbxO_3$ catalysts [6], $ZrO_2$ and $Yb_2O_3$ [7], $CeO_2$ doped with Na [8], rare earth oxide [9, 10], MgO-modified $ZrO_2$ [11] were systematically utilized for synthesis of unsaturated alcohols, and THP from 1,5-pentanediol. Gnanamani et al., reported the use of $Ga_2O_3$ doped on $CeO_2$ basic solid oxide support, as catalyst for production of mono alcohols and un saturated alcohols from 1,5-pentanediols, with improved yields [12]. Even though, few solid oxide catalysts such as $CeO_2$-based binary oxides and iron oxide accomplished dehydration of 1,6-hexanediol to useful products, not many studies addressed the aspect of its dehydration [1, 4]. Most of the reported catalysts have lower selectivity towards the desired products tetrahydropyran and oxepane from their respective alcohols [1, 4, 13, 14]. Based on different linear unsaturated products formation, the catalyst characteristics played a crucial role. While, a basic environment facilitates the alkane diols dehydration reactions, along with adequate acidic texture helps in formation of major cyclic products (cyclic ethers) [13, 14]. In the view of product selectivity, earlier reported catalysts did not encourage conversion of 1,5-PDO and 1,6-HDO *via* selective cyclic dehydration, consequently THP and oxepane yields were less than 70%. Furthermore, these catalysts were expensive, hazardous and non-biodegradable. To overcome such limitations, efficient, easily recyclable and eco-friendly alternative catalysts with higher selectivity are in demand.

Hence, we have explored for materials with catalytic properties of the solid acid oxide catalysts sustainable for prolonged time on stream measurements in the dehydration. As a result, we earlier reported the scope of activated marble waste (AMW) as a catalyst for 1,4-BDO dehydration, but it could not regulate catalytic steadiness in time-on-stream studies due to noticeable phase changes during the course of reaction [15]. To overcome the aforementioned drawbacks, we have examined another inexpensive, bio-degradable and highly selective material, the activated red brick powder as a solid acid oxide catalyst for cyclic dehydration of aliphatic alcohols. It is an eco-friendly and showed remarkable catalytic properties in 1,4-BDO dehydration [16]. In this communication we have explored the outstanding catalytic efficiency of ARB clay, in the dehydration of 1,5-PDO and 1,6-HDO into THP and oxepane respectively with superior selectivity.

Herein, we have also discussed the surface adsorptive acidic atmosphere and catalytic efficiency of commercial silica and $\alpha$-$Fe_2O_3$ catalysts for the dehydration of


https://doi.org/10.1016/j.heliyon.2019.e01212

1,5-BDO and 1,6-PDO, in addition systematically comparing with ARB clay catalytic competence. These major products formation extensively correlated with surface Lewis and Bronsted acidic sites (from Py-FT-IR) along with weak to medium acidic texture of the ARB clay catalyst (*via* $NH_3$-TPD). The kinetic reaction parameters such as, GHSV ($h^{-1}$), temperature effect, influence of Lewis and Bronsted acidic character in the product distribution, time-on-stream and comparison of catalytic activity against conventional catalysts are systematically studied and plausible reaction mechanisms were also proposed for 1,5-PDO and 1,6-HDO alcohols dehydration.

## 2. Experimental

### 2.1. Catalyst preparation

ARB clay catalyst is prepared through a simple grinding method. The red brick samples are crushed into a uniform size, washed with deionised water several times, separated into small size granules and dried at 120 °C for 24 h. The obtained powder is designated as ARB clay catalyst. Commercial silica and $\alpha$-$Fe_2O_3$ were purchased from M/s. SD-Fine (AR grade, 99.9% purity).

### 2.2. Catalyst characterization

Powder XRD measurements were carried using Rigaku diffractometer (ULTIMA-IV, 40 kV, 30 mA) with monochromatic Cuk$\alpha$ radiation. FT-IR spectra were investigated on spectrum GX spectrometer (M/s. Perkin Elmer, USA) in the scan range of 4000−400 $cm^{-1}$. SEM and EDX analysis were performed using JEOL FE-SEM-7610F to elucidate the morphology and metal composition of the catalyst. X ray fluorescence spectra carried out on (XRF, Model Bruker, SH Pioneer), X ray tube; Rh anode and operated at 4 KW. Pyridine FT-IR investigation on the pyridine adsorbed ARB clay catalyst was recorded on a Spectrum-GX spectrometer (M/s. Perkin Elmer, Germany) in the scan range 1600−1400 $cm^{-1}$. UV-Vis DRS were recorded using UV Win Lab spectrometer (M/s. Perkin Elmer, Germany) with an integrating sphere reflectance accessory in the wavelength range of 200−800 nm.

### 2.3. Catalytic activity evaluation on ARB clay, commercial silica and $\alpha$-$Fe_2O_3$ catalyst

The catalytic activity was investigated in a fixed bed down flow quartz reactor (14 mm id × 300 mm long) at atmospheric pressure in the temperature range of 300−400 °C (1,5-PDO) and 375−450 °C (1,6-HDO) with $N_2$ gas flow. Briefly, a catalyst mass of 1 g has been placed at the centre of the reactor between two quartz wool plugs and above the catalyst bed, quartz glass chips to act as a preheating zone was filled. The reactor was placed vertically inside an electrically heated tubular


https://doi.org/10.1016/j.heliyon.2019.e01212

furnace, the temperature being controlled by a temperature indicator-programmer with a K-type thermocouple. The catalyst was activated in a flow of $N_2$ gas at 450 °C for 1 h prior to the reaction. After the activation, the temperature was set up to the desired reaction environment, and the reaction was started by pumping (1,5-PDO) feed (1 $cm^3$ $h^{-1}$) by a syringe pump (M/s. B. Braun, Germany) along with $N_2$ gas (30 $cm^3$ $min^{-1}$). Whereas, aqueous solution of 1,6-HDO with the concentration of 8 mmol $h^{-1}$ (1 $cm^3$ $h^{-1}$) was fed into the reactor along with $N_2$ gas (30 $cm^3$ $min^{-1}$). The liquid effluent from the reactor out let was condensed in ice cooled trap and was analysed at regular intervals on a flame ionization detector (FID) equipped gas chromatograph (M/s. HP, USA), using a 30m wax GB capillary column.

## 3. Results and discussion

### 3.1. X-ray diffraction (XRD)

Fig. 1 illustrates the XRD patterns of fresh ARB clay along with commercial silica and α-$Fe_2O_3$ catalysts. The XRD pattern indicates the presence of crystalline $SiO_2$ in the quartz form corresponding to 2θ values at, 20.8°, 26.7°, 39.5°, 50.2° and iron oxide in the hematite form with respect to 2θ value at 33.3°. While, 2θ value at 27.9° was attributed to feldspar it was formed by the combination of calcium or

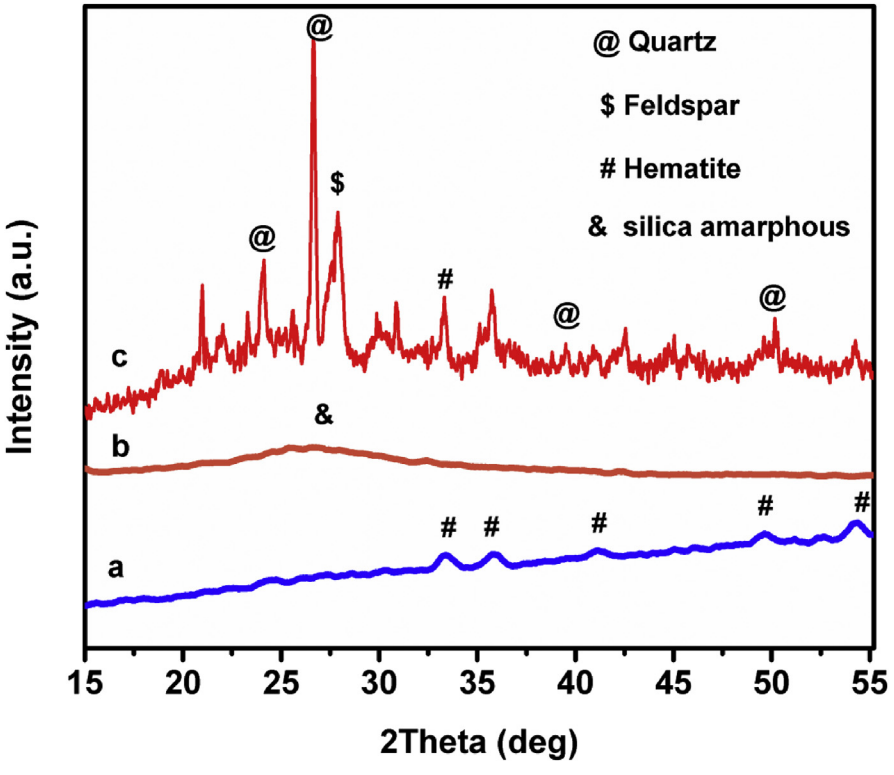


**Fig. 1.** XRD patterns of commercial (a) α-$Fe_2O_3$ (b) silica and (c) ARB clay catalysts.


https://doi.org/10.1016/j.heliyon.2019.e01212

sodium or potassium with alumino silicate [17]. In this study, we did not observe any iron silicates peak, due to presence of silica and iron oxide particles in well-dispersed manner. Herein, the patterns of commercial silica and α-$Fe_2O_3$ are illustrated. However, α-$Fe_2O_3$ displayed similar 2θ value at 33.3° pattern observed in ARB clay catalyst, but with mild intensity, which clearly indicates the amorphous nature of iron oxide particles. In addition, commercial silica also displayed broad peak in the range between 2θ values of 20−30°, thus indicating the amorphous nature of silica particles.

## 3.2. FT-IR spectra

Fig. 2, illustrates the FT-IR spectra of fresh ARB clay along with commercial silica and α-$Fe_2O_3$. The absorption bands present at 535 and 580 $cm^{-1}$ were resultant of the stretching and torsional vibrational modes of hematite Fe-O bonds in ARB clay and commercial α-$Fe_2O_3$ [18, 19]. Bands appeared at 470 and 795 $cm^{-1}$ indicate the Si-O-Si symmetric stretching vibrations. The bands around at 1097 and 940 $cm^{-1}$ are attributed to asymmetric stretching vibration of Si-O-Si and Si-OH bonds corresponding to the silica network present in ARB clay and commercial silica [20]. Moreover, 462 and 531 $cm^{-1}$ in commercial α-$Fe_2O_3$ is ascribed to oxygen coordinated with Fe metal ions (Fe-O stretching vibrations), which is clearly endorsed by existed reports [19].

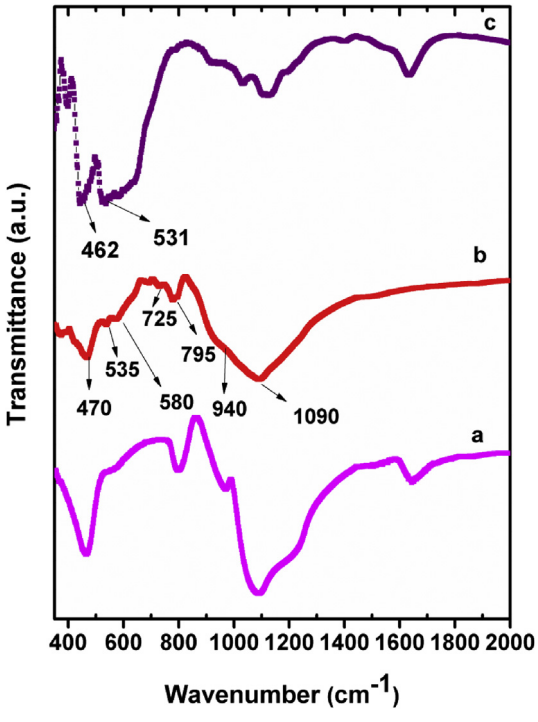


**Fig. 2.** FT-IR analysis of fresh (a) commercial silica, (b) ARB clay, (c) α-$Fe_2O_3$ catalysts.


https://doi.org/10.1016/j.heliyon.2019.e01212

### 3.3. XRF analysis

The XRF characterization of fresh and spent ARB clay catalysts evidently demonstrates the accurate weight percentage (wt%) of corresponding metals and results are summarized in Table 1. ARB clay catalyst possessed high composition of solid acidic oxides such as silica (quartz) and iron oxide (hematite) with sufficient Lewis and Bronsted acidic sites, unlike basic oxides such as feldspar, magnesium oxide and potassium oxide. ARB clay material mostly contains Si, Fe, Al, Ca, Mg and K with other inorganic metals at ppm level. A good correlation between the wt% of different metals with XRF and EDX analysis is presented in Table 1.

### 3.4. SEM-EDX

SEM images of fresh and spent ARB clay catalysts described the presence of macro pores and sheet like morphology as shown in Fig. 3a and b. The appearance of porous matrix was due to development of hematite with an alignment of uniform red Fe-rich small crystals on the surface of ARB clay catalyst. The energy dispersive X-ray analysis of (3c) fresh and (3d) used ARB clay catalysts confirms the major presence of Si, Fe, Al elements and minor quantities of Ca, K and Mg as tabulated in Table 1.

### 3.5. $NH_3$-temperature programmed desorption (TPD)

$NH_3$-TPD measurements provide the distribution and strength of acidic sites in the catalysts. Fig. 4 illustrates the TPD profiles of commercial silica, $\alpha$-$Fe_2O_3$ and ARB clay catalysts. The $NH_3$ desorption peak around 100−250 °C in commercial silica reveals the existence of weak acidic sites comparison to ARB clay catalyst. In case of $\alpha$-$Fe_2O_3$, desorption peaks in the range of 500−750 °C indicates the presence of strong acidic sites. Commercial silica exhibits moderate and (73%) 1,5-PDO and (79%) 1,6-HDO conversion due to weak acidic sites compared to $\alpha$-$Fe_2O_3$ which showed better (100%) 1,5-PDO and (100%) 1,6-HDO conversion

**Table 1.** Analysis (wt%) of fresh and spent ARB clay catalysts.

| Metal | Wt% (XRF) | | Wt% (EDX) |
|---|---|---|---|
| | Fresh ARB | Used ARB | Fresh ARB |
| Fe | 5.29 | 5.24 | 5.27 |
| Si | 12.49 | 12.42 | 12.35 |
| Al | 5.18 | 5.14 | 5.22 |
| K | 1.23 | 1.21 | 1.42 |
| Ca | 2.84 | 2.83 | 2.99 |
| Mg | 0.14 | 0.11 | 0.12 |


https://doi.org/10.1016/j.heliyon.2019.e01212

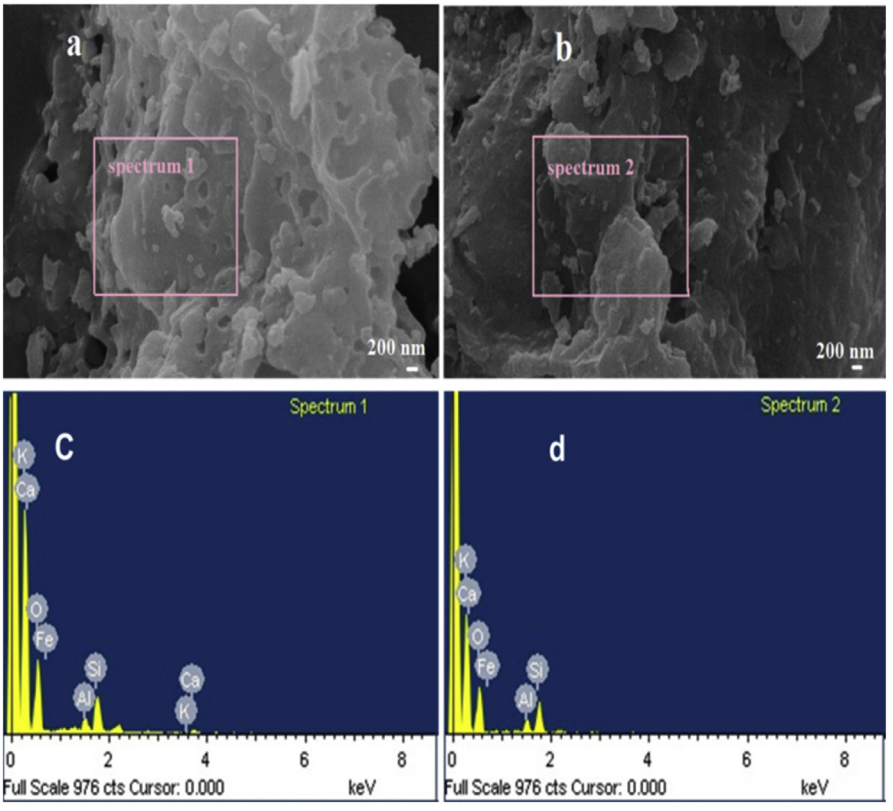


**Fig. 3.** SEM-EDX patterns of (a, c) fresh and (b, d) spent ARB clay catalysts.

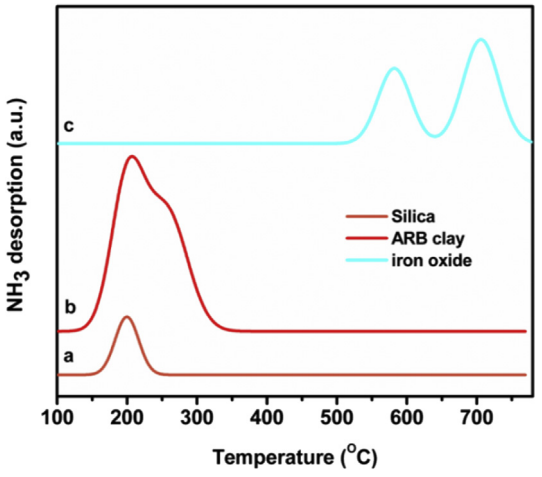


**Fig. 4.** $NH_3$-TPD patterns of (a) commercial silica, (b) ARB clay, and (c) $\alpha$-$Fe_2O_3$ catalysts.

with strong acidic sites. However, there has been drastic decline in (39%) THP and (~30%) oxepane selectivity on commercial $\alpha$-$Fe_2O_3$ and silica catalysts. Whereas ARB clay catalyst, high intense desorption peak approximately 180 °C and a shoulder peak at 275 °C with maximum $NH_3$ consumption correlated to the weak and medium acidic sites (Fig. 4).


https://doi.org/10.1016/j.heliyon.2019.e01212

Thus, the co-existence of both weak and medium acidic sites in ARB clay catalyst has strongly enhanced the dehydration catalytic efficiency of 1,5-PDO and 1,6-HDO towards better yields of THP and oxepane (as depicted in Tables 3 and 4). This clearly evidences the existence of synergistic effect of Fe on Si oxide species or combinational catalytic efficiency in the ARB clay catalyst offering to full 100% conversion of 1,5-PDO and 1,6-HDO.

## 3.6. Pyridine FT-IR

Pyridine FT-IR elucidates the nature of acidic sites present in the catalyst. The pyridine FT-IR spectra of fresh ARB clay, commercial silica and $\alpha$-$Fe_2O_3$ catalysts were presented in Fig. 5. Obviously, two weak bands at 1450 and 1472 $cm^{-1}$ for ARB clay catalyst was described to pyridine adsorbed onto hematite $Fe^{3+}$ Lewis acidic species [21, 22], while band at 1492 $cm^{-1}$ was pertaining to pyridine adsorbed onto both Lewis and Bronsted acidic clusters [23]. A strong band at 1540 $cm^{-1}$ was ascribed to noticeable Bronsted acidic [24] moieties (silanol) became wider and high intense remain as similar intense in ARB. In addition, adsorption band at 1575−1590 $cm^{-1}$ ascribed to Lewis acidic sites in the ARB clay catalyst [25]. Herein, commercial $\alpha$-$Fe_2O_3$ catalyst simply displayed Lewis acidic sites in the range of

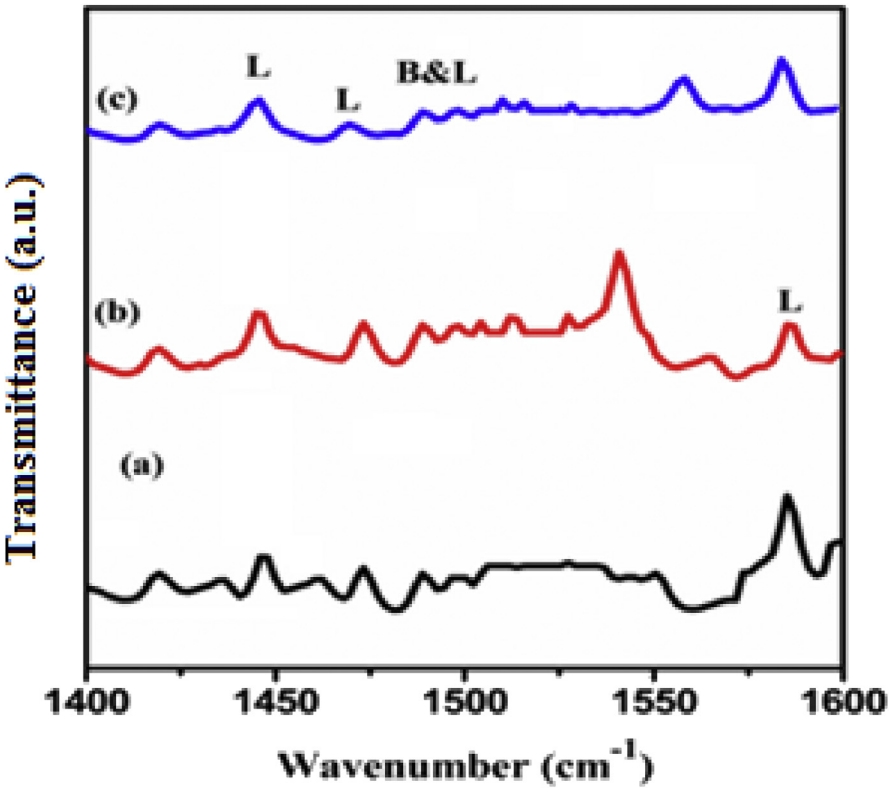


**Fig. 5.** Pyridine FT-IR patterns of (a) commercial $\alpha$-$Fe_2O_3$, (b) ARB clay, and (c) commercial silica catalysts.


https://doi.org/10.1016/j.heliyon.2019.e01212

1575−1590 $cm^{-1}$ those were vital responsible in dehydration, isomerization, hydrogenation as well as dehydrogenation products distribution. As a result, higher fraction of unwanted products (i.e, 2,3-dihydropyran, 4-pentene-1-ol, and 5-nonanone from 1,5-PDO and cyclopentanone, 1-hexanol, 6-undecanone and 5-hexene-1-ol from 1,6-HDO) obtained over α-$Fe_2O_3$ catalyst. In contrast with α-$Fe_2O_3$, commercial silica catalyst exhibited low intense Lewis acidic sites [26, 27] as a result lower 1,5-PDO and 1,6-HDO conversions, but better product selectivity achieved like, 63% THP and 30% oxepane respectively. It seems, Bronsted acidic sites were quantitatively more compared to Lewis acidic sites in the ARB clay catalyst. The synergistic effect of both Bronsted and Lewis acidity as well as weak to mild acidic nature was majorly regulate the selective intramolecular cyclized dehydration of 1,5-PDO to THP 1,6-HDO to oxepane, with small fraction of side products.

In addition, small fractions of Bronsted acidic sites were observed in commercial silica catalyst, due to lesser number of surface silanol groups, whereas the Lewis acidic sites displayed by α-$Fe_2O_3$ were reason for poor catalytic activity in terms of poor THP and oxepane selectivity.

### 3.7. UV-vis DRS spectra

Fig. 6 depicts the UV-Vis DRS of fresh and spent ARB clay catalyst. A strong absorption band with maxima at 250 nm corresponds to ligand to metal charge transfer character that involves $O^{-2}$ to isolated four coordinated $Fe^{+3}$ ions.

In addition, a broad absorption band in the range of 500−550 nm represents the surplus Fe atoms in hematite domain of ARB clay catalyst [28]. Existing literature provides little explanation regarding the red brick clay materials as catalysts.

## 4. Analysis

### 4.1. Temperature effect on dehydration of 1,5-PDO and 1,6-HDO over ARB clay, commercial silica and α-$Fe_2O_3$ catalysts

The 1,5-PDO dehydration is reported to give tetrahydropyran (THP), δ-valerolactone (DVL) as major compounds, along with 1,4-pentadiene, pentanal, 1-pentanol, 4-penten-1-ol, 2,3-dihydropyran, 5-nonanone and 5-hydroxypentanal as minor products [8, 9, 10, 11, 12]. In the 1,6-HDO dehydration reactions, typical products were 5-hexene-1-ol, cyclopentanone, 6-undecanone, 1-hexanol, hexanal, cyclopenetnone and oxepane [4, 13, 14]. All the above, products formation considerably depends on catalyst acid-basic nature and reaction operation conditions.

Tables 2 and 3, along with Fig. 7a and b summarise the results of conversion of 1,5-PDO and 1,6-HDO to respective products at different temperatures over ARB clay, commercial silica and α-$Fe_2O_3$ catalysts. In the present study, using ARB clay, we


https://doi.org/10.1016/j.heliyon.2019.e01212

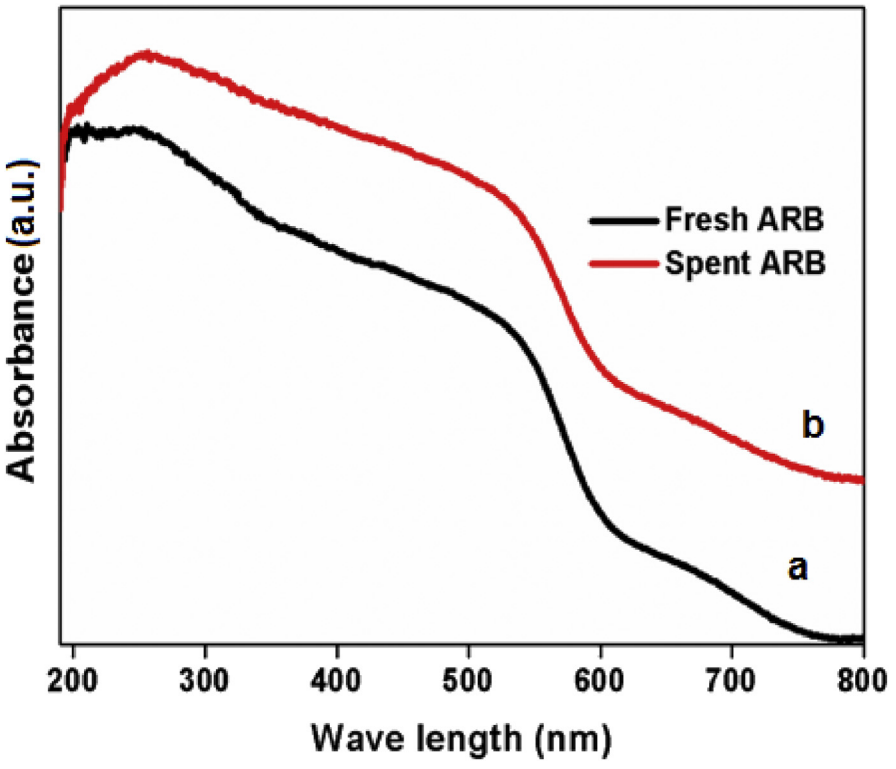


**Fig. 6.** UV-Vis DRS patterns of (a) fresh and (b) spent ARB clay catalysts.

have obtained the desired products with higher selectivity and in the dehydration of 1,5-PDO and 1,6-HDO in comparison with commercial α-$Fe_2O_3$ and silica as catalysts. In general, the conversion of alkane diols (Thermodynamic reactions) increased with increasing the reaction temperature. Commercial silica catalyst achieved low conversion at mild temperature (at 300−350 °C), while at high temperature i.e., at 375 °C 1,5-PDO attained 73% and at 425 °C 1,6-HDO gave 79% conversion with beneficial selectivity to 63% THP and 30% oxepane respectively

**Table 2.** 1,6-HDO conversion over ARB clay, commercial silica and α-$Fe_2O_3$ catalysts.

| Catalyst | Conversion (%) | Oxepane selectivity (%)[a] | Others selectivity (%)[b,c,d] |
|---|---|---|---|
| ARB | 100 | 89 | [b]11 |
| Silica | 79 | 30 | [c]70 |
| α-Iron oxide | 100 | 43 | [d]57 |

**Reaction conditions:** Temperature; 425 °C, 1,6-HDO feed flow 8 mmol $h^1$ (1 $cm^3$ $h^{-1}$), GHSV 753 $h^{-1}$ with respect to nitrogen, 1 atm. pressure, 1g catalyst.

[a] **Selectivity (%):** Oxepan.

[b] **Selectivity (%):** 1,2-cyclohexanediol and 6-undecanone.

[c] **Selectivity (%):** 5-hexene-1-ol, 4-hexene-1-ol and 5-hexenal.

[d] **Selectivity (%):** cyclopentanone, 6-undecanone and 2-cyclopenten-1-one.


https://doi.org/10.1016/j.heliyon.2019.e01212

**Table 3.** 1,5-PDO conversion over ARB clay, commercial silica and α-$Fe_2O_3$ catalysts.

| Catalyst | Conversion (%) | THP selectivity (%)[a] | Others selectivity (%)[b,c,d] |
|---|---|---|---|
| ARB | 100 | 82 | [b]18 |
| Silica | 73 | 63 | [c]37 |
| α-Iron oxide | 100 | 39 | [d]61 |

**Reaction conditions:** Temperature; 375 °C, 1,5-PDO feed flow; 1 mL/h, GHSV 762 $h^{-1}$ with respect to nitrogen, 1 atm. pressure, 1 g catalyst.

[a] **Selectivity (%)** Tetrahydropyran.

[b] **Selectivity (%):** 2,3-dihydropyran, pentanal, 5-nonanone, and 4-penten-1-ol.

[c] **Selectivity (%):** 2,3-dihydropyran.

[d] **Selectivity (%):** 4-penten-1-ol, 5-nonanone, 2,3-dihydropyran and pentanal.

(Tables 2 and 3). The dehydration reaction mechanism on commercial α-$Fe_2O_3$ catalyst significantly differs from commercial silica and ARB clay catalysts.

Hence, 1,5-PDO and 1,6-HDO dehydration reaction on commercial α-$Fe_2O_3$ catalyst tend to majorly produce dehydration, isomerized, aldol cyclized products, hydrogenation and dehydrogenation products rather than desired products (i.e., THP and oxepane) revealed in Tables 2 and 3. Moreover, trace level intermolecular dehydration products, such as, 5-nonanone and 6-undecanone was also observed at high temperatures as depicted in Tables 2 and 3. This is because of the adverse surface acidic texture (see $NH_3$-TPD pattern) and Lewis acidic sites (see Py-FT-IR, Fig. 5) on α-$Fe_2O_3$ catalyst compared to that of commercial silica (Lewis acidic sites only) and ARB clay catalyst (Lewis and Bronsted acidic sites). While, ARB clay catalyst with silica and iron oxides, the synergistic Lewis and Bronsted acidic properties majorly offered intramolecular dehydration. Thereby, 100% conversion of 1,5 and 1,6-alkanediols with high product selectivity and trace concentrations of other intermolecular dehydration compounds, such as 5-nonanone and 6-undecanone. The minor products are due to, iron oxide particles in ARB clay catalyst contributing to small fraction of intermolecular dehydration products during the course of temperature effect. Commercial silica catalyst merely afforded competent intramolecular dehydration products selectivity such as oxepane and tetrahydropyran along with unsaturated diols. The commercial silica and ARB clay catalysts showed 63% and 82% selectivity towards THP at 375 °C. Striking difference was observed for oxepane selectivity, 30% with silica compared to 89% attained with ARB clay (425 °C). High reaction temperature also diminishes the efficiency of commercial silica (intramolecular dehydration) and α-$Fe_2O_3$ (intermolecular dehydration) catalysts leading to rise in contribution of side products.

It was due to mild thermal and mechanical properties together with adsorption of more number of $H_2O$ molecules during the dehydration thereby accumulate high carbon deposits.


https://doi.org/10.1016/j.heliyon.2019.e01212

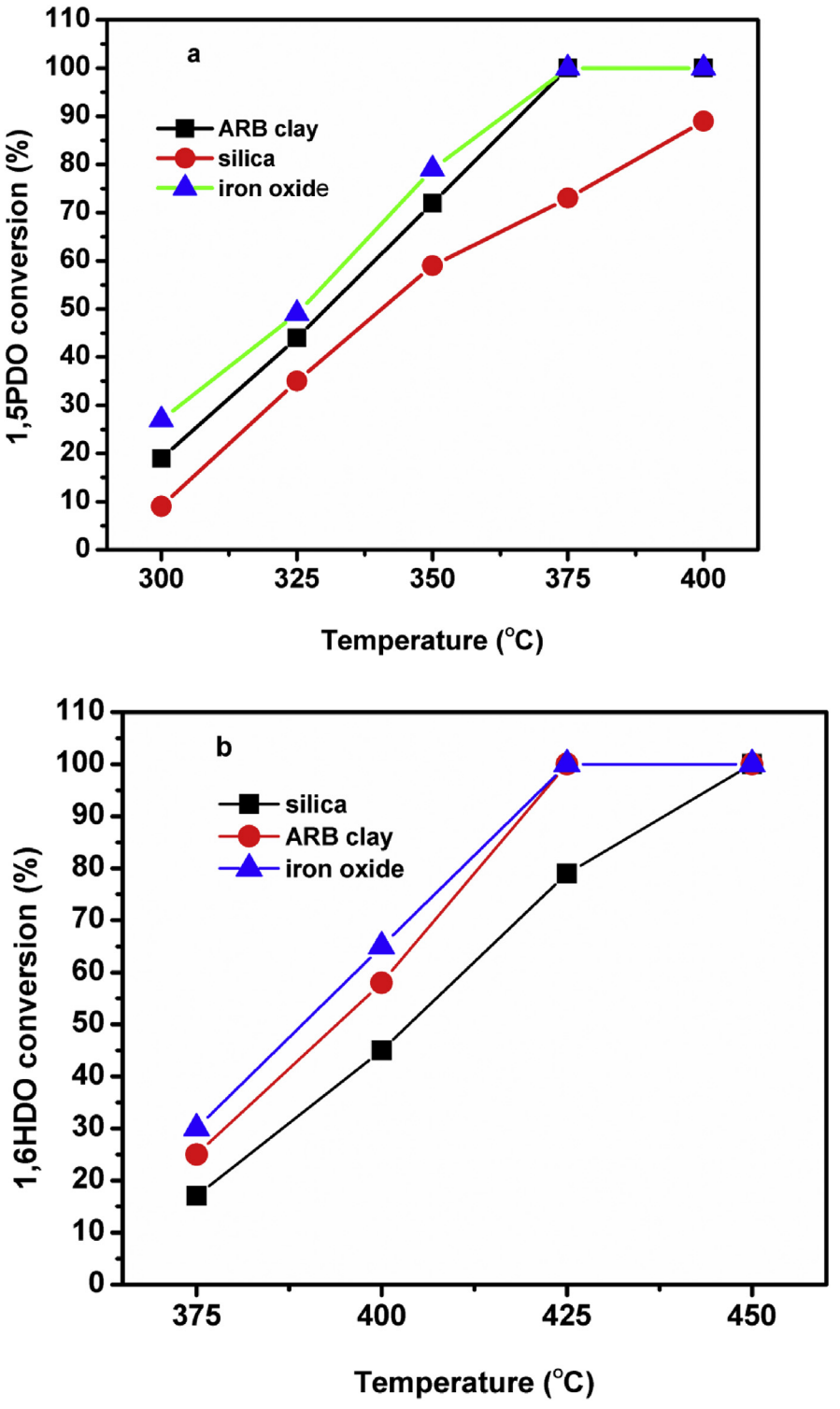


**Fig. 7.** a and b. Temperature effect on conversion of 1,5-PDO and 1,6-HDO over ARB clay, commercial silica and $\alpha$-$Fe_2O_3$ catalysts. [a]Reaction conditions; Temperature; 300−400 °C, 1,5-PDO feed flow; 1 mL/h, GHSV 762 $h^{-1}$ with respect to nitrogen, 1 atm. pressure, 1g catalyst. [b]Reaction conditions; Temperature; 375−450 °C, 1,6-HDO feed flow; 8 mmol/h (1 $cm^3$ $h^{-1}$), GHSV 753 $h^{-1}$ with respect to nitrogen, 1 atm. pressure, 1g catalyst.


https://doi.org/10.1016/j.heliyon.2019.e01212

Under similar reaction conditions, 82% THP and 89% oxepane formation rate dramatically improved over ARB clay catalyst, along with conversion of 100% 1,5-PDO and 1,6-HDO. As per improved catalytic action, it was found that ARB clay catalyst displayed higher desired product yields at all reaction temperatures irrespective of 1,5-PDO and 1,6-HDO reactants concentration. It was due to synergistic Lewis and Bronsted acidic properties of $Si^{+4}$ and $Fe^{+3}$ species responsible in the intramolecular dehydration of alcohols. For this reason, ARB clay catalyst has extensively been suppressed the unwanted products formation in comparison to commercial silica and $\alpha$-$Fe_2O_3$ catalysts. Based on our speculation on higher catalytic activity, ARB clay catalyst possessed silica species are played a major role in marvellous products selectivity. This noticeably endorsed by optimal acidic nature of iron oxide particles in ARB clay catalyst. During the temperature effect, 1,5-PDO and 1,6-HDO conversion increases with increasing the reaction temperature, meanwhile THP and oxepane selectivity reached the highest at 375 °C and 425 °C, then calmed down after that. Instead, higher fraction of by-products such as, pentanal, 1-pentanol, 5-nonanone and 5-hydroxypentanal are produced from 1,5-PDO, preferentially at high temperatures on commercial silica and $\alpha$-$Fe_2O_3$ catalysts. Whereas, 5-hexene-1-ol, 2-cyclopenten-1-one, 6-undecanone and cyclopentanone compounds were competently observed in the 1,6-HDO dehydration on commercial silica, and $\alpha$-$Fe_2O_3$ catalysts. In contrast, weak to mild acidic nature possessed ARB clay catalyst afforded lesser fraction of 5-nonanone and 6-undecanone was observed in the case of 1,5-PDO and 1,6-HDO dehydration. This is due to predominant intramolecular condensation phenomenon rather than intermolecular condensation. According to, impressive 1,5 and 1,6-alkanediols conversion and selectivity to oxepane and THP, the most preferable reaction temperature was 375 °C and 425 °C over ARB clay, commercial silica, and $\alpha$-$Fe_2O_3$ catalysts Table 4. Thereby, ARB clay catalytic activity afforded 100% conversion of 1,5-PDO (1 mL/h, 1,5-PDO) with 82% THP selectivity at 375 °C and 100% conversion of 1,6-HDO (8 mmol/h, 1,6-HDO) with 89% oxepane at 425 °C until 12 h time on stream. The effect of contact time in terms of GHSV over the catalytic dehydration is well summarized in Table 4.

## 4.2. Effect of $N_2$ gas hourly space velocity (GHSV) on catalytic activity and product distribution

In this context, the crucial influence GHSV of $N_2$ gas flow, in regulation of 1,6-HDO and 1,5-PDO conversion and product selectivity over ARB clay, commercial silica and $\alpha$-$Fe_2O_3$ catalysts is showed in Table 4. Thus $N_2$ flow rate of 1094 (1,6-HDO) and 1103 $h^{-1}$ (1,5-PDO) was not promising due to little contact time of reactants with active metal surface of the catalyst, as a result <80% 1,6-HDO and 1,5-PDO conversion. The 753 (1,6-HDO) and 762 $h^{-1}$ (1,5-PDO) $N_2$ flow rate was good with 100% 1,6-HDO and 1,5-PDO conversion due to excellent adsorptive interaction


https://doi.org/10.1016/j.heliyon.2019.e01212

**Table 4.** GHSV effect on 1,6-HDO and 1,5-PDO conversion with ARB clay, commercial silica and α-$Fe_2O_3$ catalysts.

| Catalyst | [1]$N_2$ GHSV/$h^{-1}$ | [a]1,6-HDO conversion (%) | [b]Oxepane selectivity (%) | [2]$N_2$ GHSV/$h^{-1}$ | [c]1,5-PDO conversion (%) | [d]THP selectivity (%) |
|---|---|---|---|---|---|---|
| ARB | 412 | 90 | 74 | 422 | 94 | 71 |
| | 753 | 100 | 89 | 762 | 100 | 82 |
| Silica | 1094 | 78 | 87 | 1103 | 72 | 80 |
| | 412 | 71 | 22 | 422 | 53 | 51 |
| α-$Fe_2O_3$ | 753 | 79 | 30 | 762 | 73 | 63 |
| | 1094 | 54 | 31 | 1103 | 45 | 60 |
| | 412 | 100 | 38 | 422 | 100 | 32 |
| | 753 | 100 | 43 | 762 | 100 | 39 |
| | 1094 | 86 | 52 | 1103 | 79 | 41 |

[1]**Reaction conditions:** Temperature; 425 °C, 1,6-HDO feed flow; 8 mmol $h^1$ (1 $cm^3$ $h^{-1}$), $N_2$ gas flow; 15, 30 and 45 ml/min, 1 atm. pressure, 1g catalyst.
[2]**Reaction conditions:** Temperature; 375 °C, 1,5-PDO feed flow; 1 ml $h^{-1}$, $N_2$ gas flow; 15, 30 and 45 ml/min 1 atm. pressure, 1g catalyst.
[a] **Conversion (%)**; 1,6-HDO.
[b] **Selectivity (%):** Oxepane.
[c] **Conversion (%):** 1,5-PDO.
[d] **Selectivity (%):** THP.

between reactants and Lewis and Bronsted acidic sites of the ARB clay catalyst. Thereby, this reaction condition accomplished optimum oxepane and THP selectivity. However, commercial silica and α-$Fe_2O_3$ catalysts showed lower 1,5-PDO and 1,6-HDO conversions as well as product selectivity under optimal and other GHSV conditions (Table 4). At 412 (1,6-HDO) and 422 $h^{-1}$ (1,5-PDO) $N_2$ GHSV flow rate afforded better conversions for 1,6-HDO and 1,5-PDO with ARB clay and α-$Fe_2O_3$ catalysts, still low conversions with silica, but selectivity's with silica and α-$Fe_2O_3$ for desired products were significantly low. Thus owing to, higher residence time of reactants commercial silica and α-$Fe_2O_3$ catalysts lead to adverse products selectivity as shown in Table 4. While $N_2$ GHSV flow rates and temperatures had less influence on the selectivity of products on ARB clay catalyst, it influenced the product profile significantly with commercial silica and α-$Fe_2O_3$ catalysts.

In conclusion, optimal $N_2$ gas GHSV flow improved the 1,5 and 1,6-alkanediols conversion as well as product selectivity on ARB clay catalyst minimising the side reactions.

## 4.3. Influence of 1,6-HDO concentration on product selectivity and conversion

The 1,6-HDO concentration key factor in the conversion as well as product selectivity as depicted in Table 5. Here in, we have investigated the 1, 2, 4, 6 and 8 mmol $h^{-1}$ 1,6-HDO concentrations over the ARB clay, commercial silica and


https://doi.org/10.1016/j.heliyon.2019.e01212

**Table 5.** Effect of 1,6-HDO concentration on product selectivity and conversion on ARB clay catalyst.

| [1]1,6-HDO Concentration | [2]Temperature °C | [a]1,6-HDO conversion (%) | [b]Oxepane selectivity (%) | [c]Others selectivity (%) |
|---|---|---|---|---|
| 1 mmol $h^{-1}$ | 400 | 100 | 89 | 11 |
| | 425 | 100 | 88 | 12 |
| 2 mmol $h^{-1}$ | 450 | 100 | 80 | 20 |
| | 400 | 100 | 89 | 11 |
| | 425 | 100 | 87 | 13 |
| | 450 | 100 | 78 | 22 |
| 4 mmol $h^{-1}$ | 400 | 89 | 87 | 13 |
| | 425 | 100 | 86 | 14 |
| | 450 | 100 | 73 | 17 |
| 6 mmol $h^{-1}$ | 400 | 81 | 88 | 12 |
| | 425 | 100 | 83 | 17 |
| | 450 | 100 | 69 | 31 |
| 8 mmol $h^{-1}$ | 400 | 73 | 87 | 13 |
| | 425 | 100 | 89 | 11 |
| | 450 | 100 | 62 | 38 |

[1,2]**Reaction conditions:** Temperature; 400, 425 and 450 °C, 1,6-HDO feed flow; 1, 2, 4, 6 and 8 mmol $h^{-1}$ (1 $cm^3$ $h^{-1}$), $N_2$ gas flow; 30 ml/min, 1 atm. pressure, 1 g catalyst.

[a] **Conversion;** 1,6-HDO.

[b] **Selectivity;** Oxepane.

[c] **Others selectivity (%):** 6-undecanone, and 1,2-cyclohexanediol.

iron oxide catalysts at optimal reaction conditions. Amongst all concentrations, 1 mmol $h^{-1}$ achieved 100% conversion. Then, 2 mmol $h^{-1}$ also attained 100% conversion similar selectivity catalytic results with desired products. While 4 mmol/h recorded a marginal decrease in 1,6-HDO conversion without significant changes in the product selectivity, thus results in insufficient active sites with increasing the reactant 1,6-HDO concentration and reaction temperature. Then 6 mmol $h^{-1}$ and 8 mmol $h^{-1}$ 1,6-HDO concentration also displayed maximum conversion at high temperatures, but selectivity decreased. At high temperature 450 °C, the 1,6-HDO dehydration preferably formed intermolecular and intramolecular dehydration products irrespective of reactant concentration (Table 5). Mild temperatures (375 and 425 °C) offered better product selectivity along with good 1,6-HDO conversion. The formation of intermolecular products such as, 5-nonanone and 6-undecanone at high temperature was clearly endorsed by literature study [13, 14].

Moreover, commercial $\alpha$-$Fe_2O_3$ and silica catalysts were also catalyzed the above mentioned 8 mmol/h 1,6-HDO concentrations as shown in Table 6.

While, commercial $\alpha$-iron oxide had kept similar trend in 1,6-HDO conversions at all concentrations as observed on ARB clay catalyst, however adverse product


https://doi.org/10.1016/j.heliyon.2019.e01212

**Table 6.** Effect of 1,6-HDO concentration on product selectivity and conversion over commercial silica and α-iron oxide catalysts.

| Catalyst | [1]1,6-HDO concentration | [2]Temperature (°C) | [a]1,6-HDO conversion (%) | [b]Oxepane selectivity (%) | [c]Others selectivity (%) |
|---|---|---|---|---|---|
| Silica | 8 mmol/h | 400 | 58 | 35 | [b]70 |
| | 8 mmol/h | 425 | 79 | 30 | [b]72 |
| α-$Fe_2O_3$ | 8 mmol/h | 450 | 85 | 21 | [b]79 |
| | 8 mmol/h | 400 | 94 | 51 | [c]49 |
| | 8 mmol/h | 425 | 100 | 43 | [c]57 |
| | 8 mmol/h | 450 | 100 | 27 | [c]73 |

[1,2]**Reaction conditions:** Temperature; 400, 425 and 450 °C, 1,6-HDO feed flow; 8 mmol $h^{-1}$ (1 $cm^3$ $h^{-1}$), $N_2$ gas flow; 30 ml/min, 1 atm. pressure, 1 g catalyst.

[a] **Conversion (%)**: 1,6-HDO.

[b] **Others selectivity (%):** 5-pentenal, 4-penten-1-ol and 5-hexene-1-ol.

[c] **Others selectivity (%):** cyclopentanone, 2-cyclopenten-1-one, and 6-undecanone.

contribution due to more number of acidic sites. In addition, commercial silica catalyst also represented the worst 1,6-HDO conversion and selective products owing to low acidic sites present on the surface of the catalyst.

## 4.4. Time-on-stream activity on ARB clay, commercial silica and α-$Fe_2O_3$ catalysts

The selective formation of THP and oxepane from 1,5-BDO and 1,6-PDO generally depends on reaction temperature (Thermodynamic reactions) along with different acidic nature of the catalyst. ARB clay catalyst clearly revels the increases in weak to mild acidic scenario, which is unique role for selective production of 82% THP and 89% oxepane during the course of time-on-stream, but not suitable for higher 4-pentene-1-ol, 5H1OL, cyclopentanone and other side products. Over ARB clay catalyst, no changesare observed in 1,5, and 1,6-alkanediols conversion and desired product selectivity due to more hydrophobic nature of silica particles [29]. Moreover, the catalytic activity of synergistic Lewis and Bronsted acidic sites on ARB clay did not decay fast. A smooth decrement in activity, thereby maintained sustained selective production of THP with a small fraction of side products generation as depicted in Figs. 8 and 9.

A small fraction of Lewis acidic sites and surface acidic sites (from Py-FT-IR and $NH_3$-TPD patterns) were investigated in commercial silica, whereas α-iron oxide catalysts promptly exhibited more quantity of Lewis acidic texture detected by $NH_3$-TPD and Py-FT-IR patterns in Figs. 4 and 5.

Judging from the formation rate of 4-pentene-1-ol, cyclopentanone, cyclopentene-1-one, 5-nonanone, 6-undecanone, 2,3-dihydropyran, 5-H1OL, and other by-products there was no similar trend observed between commercial silica and α-


https://doi.org/10.1016/j.heliyon.2019.e01212

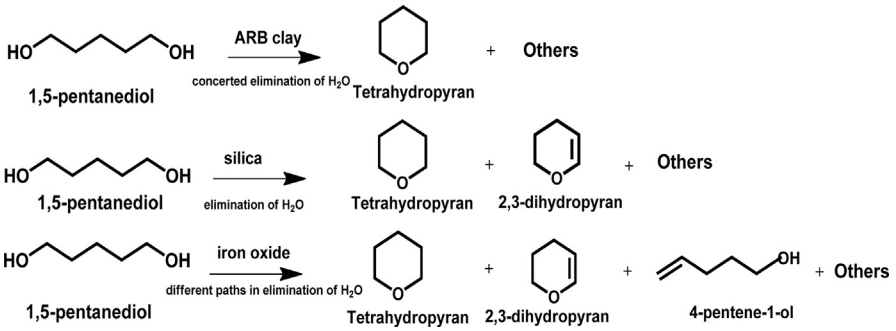


**Fig. 8.** 1,5-PDO dehydration procedure on ARB clay, commercial silica and α-$Fe_2O_3$ catalysts.

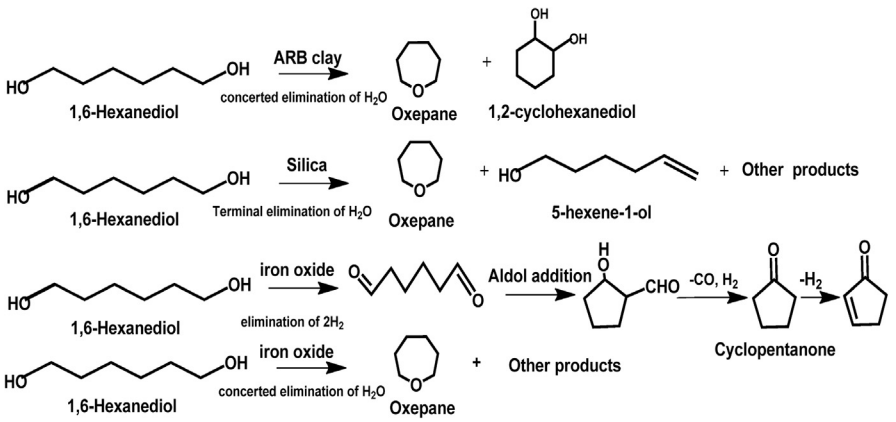


**Fig. 9.** 1,6-HDO dehydration procedure on ARB clay, commercial silica and α-$Fe_2O_3$ catalysts.

$Fe_2O_3$ catalysts in the dehydration of 1,5 and 1,6-alkanediols (Figs. 8 and 9). Though, commercial silica catalyst displayed mild 73% 1,5-PDO and 79% 1,6-HDO conversions along with optimal selectivity of useful products (63% THP and 30% oxepane) until 12 h time-on-stream in shown in Figs. 10, 11, 12, and 13. Over the commercial silica catalyst, time-on-stream was decreased smoothly passing the process time owing to hydrophobic nature of silica particles, which apparently impede the higher adsorption of water molecules. The strong acidic atmosphere possessed α-$Fe_2O_3$ catalyst typically increases the formation of side product distribution as observed in the literature [4, 13, 14]. This results in decrease in desired product yields i.e., 39% THP and 43% oxepane together with sharp decrement in time-on-stream study. At initial hours of time-on-stream thus 1,5-PDO and 1,6-HDO conversion was very much high (100%), and then significant decline to 59% and 65 % at 12 h over commercial α-$Fe_2O_3$ catalyst as shown in Figs. 10 and 11. It was due to, mild thermal and mechanical stability thereby accumulation of carbon deposits. In contrast, no significant changes were observed in the desired products distribution as well as 1,5 and 1,6-alkanediol conversion till end of the reaction over ARB clay catalyst and greatly avoid the coke deposition, evidence from CHNS and TGA analysis is


https://doi.org/10.1016/j.heliyon.2019.e01212

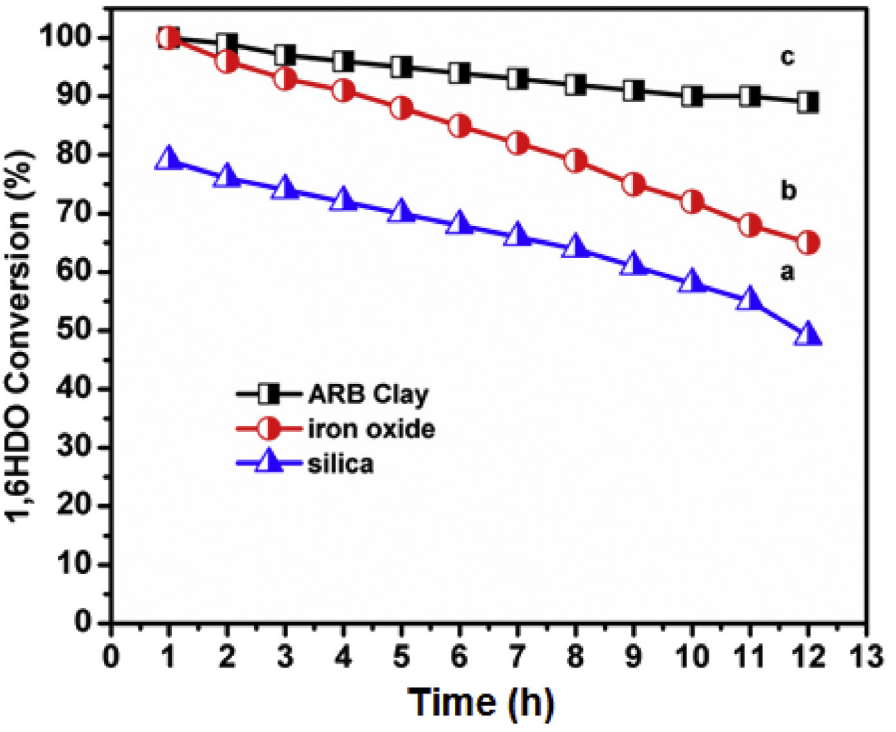


**Fig. 10.** Conversion of 1,6-HDO on (a) α-$Fe_2O_3$ (b) commercial silica (c) ARB clay catalysts. Reaction conditions; temperature; 425 °C, 1,6-HDO feed flow; 8 mmol $h^1$ (1 $cm^3$ $h^{-1}$), GHSV 753 $h^{-1}$ with respect to nitrogen flow, 1 atm. pressure, 1 g catalyst.

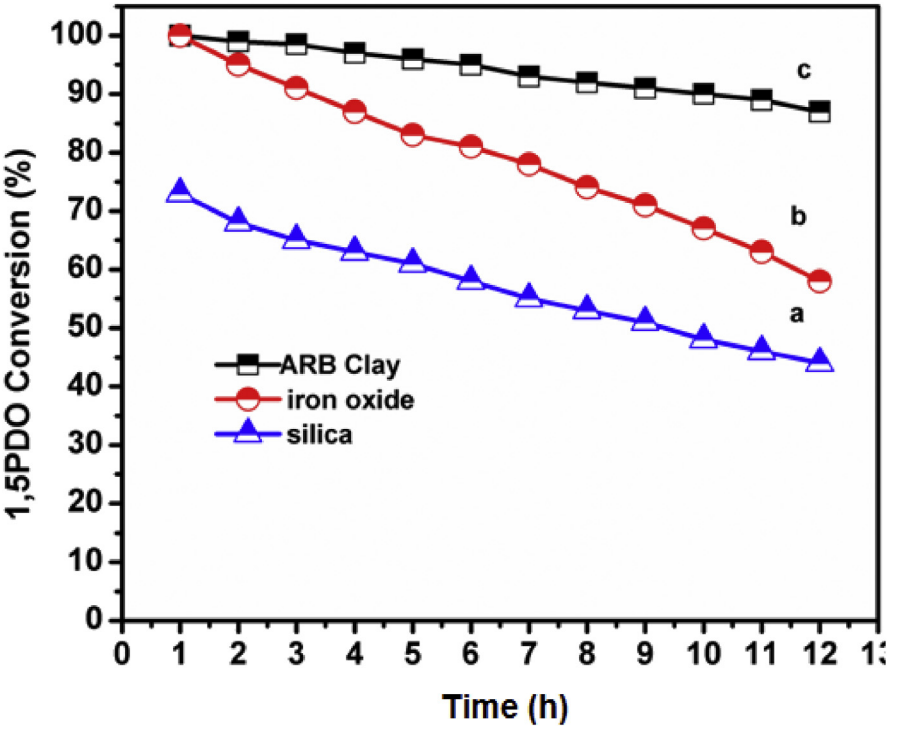


**Fig. 11.** Conversion of 1,5-PDO on (a) α-$Fe_2O_3$(b) commercial silica (c) ARB clay catalysts. Reaction conditions; temperature; 375 °C, 1,5-PDO feed flow; (1 $cm^3$ $h^{-1}$), GHSV 762 $h^{-1}$ with respect to nitrogen flow, 1 atm. pressure, 1g catalyst.


https://doi.org/10.1016/j.heliyon.2019.e01212

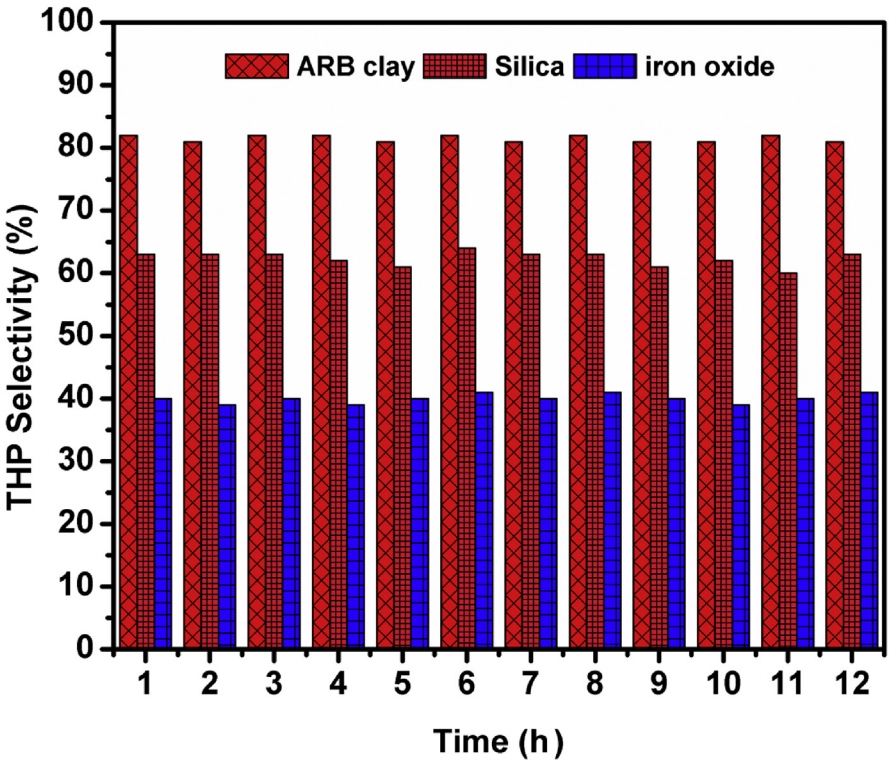


**Fig. 12.** THP selectivity on ARB clay, commercial silica and $\alpha$-$Fe_2O_3$ catalysts. Reaction conditions; temperature; 375 °C, 1,5-PDO feed flow; (1 $cm^3$ $h^{-1}$), GHSV 762 $h^{-1}$ with respect to nitrogen, 1 atm. pressure, 1 g catalyst.

not mentioned in the manuscript. Herein, major products selectivity to cyclic ethers (i.e., THP and oxepane) typically depends on advantageous adsorption of aliphatic alcohols on Lewis and Bronsted acidic sites of the ARB clay catalyst [16]. The optimal Lewis and Bronsted acidic nature in the ARB clay catalyst evidently provide the cyclised reaction mechanism for maximum THP and oxepane yields (see Figs. 8 and 9). As a result, ARB clay catalyst displayed quite remarkable surface acidic environment in comparison to commercial silica and $\alpha$-$Fe_2O_3$ catalysts. As described in the previous report [7], the acidic solid oxide catalyst that $SiO_2$-$Al_2O_3$ displayed superior 1,6-HDO and 1,5-PDO conversion and desired products selectivity for oxepane and THP rather than 5-H1OL, cyclopentene-1-one, 2,3-dihydropyran, cyclopentanone and 4-pentene-1-ol. On the other hand, the oxepane and THP selectivity obviously declined by doping basic metal oxides such as $Na_2O$, CaO, $K_2O$, SrO, MgO, $Li_2O$, and BaO respectively. It is reasonable that the selective dehydration of 1,5-PDO and 1,6-HDO into 4-pentene-1-ol and 5-H1OL considerably needed some extent mild basic sites [8, 12].

The mechanism of THP and oxepane production over the ARB clay catalyst should also be predictable as acid concerted bidentate coordination, in which


https://doi.org/10.1016/j.heliyon.2019.e01212

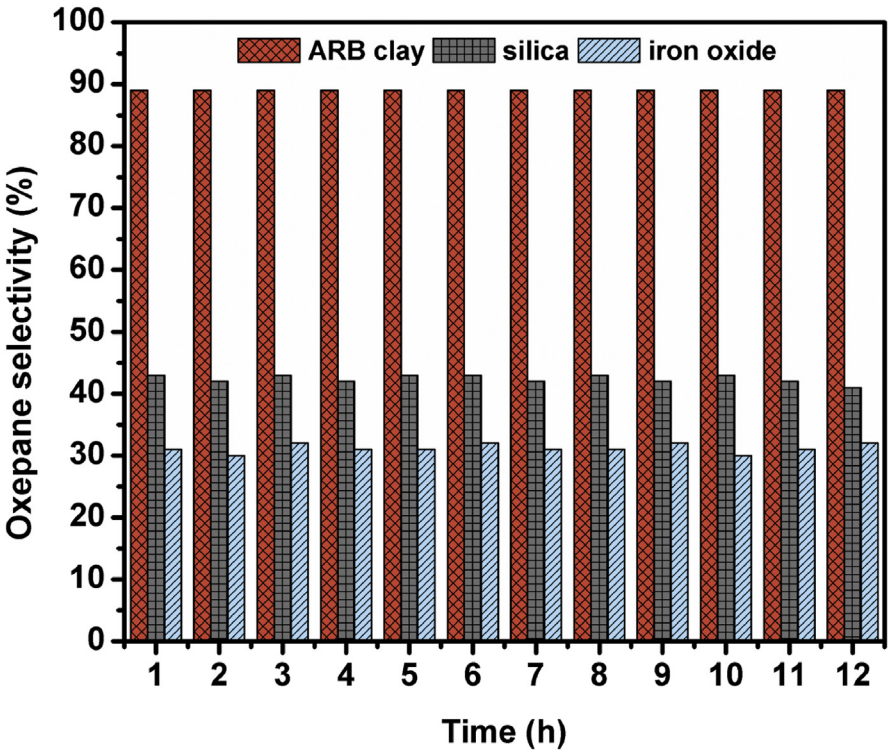


**Fig. 13.** Oxepane selectivity on ARB clay, commercial silica and α-$Fe_2O_3$ catalysts. Reaction conditions: Temperature; 425 °C, 1,6-HDO feed flow; 8 mmol $h^1$ (1 $cm^3$ $h^{-1}$), GHSV 753 $h^{-1}$ with respect to nitrogen, 1 atm. pressure, 1 g catalyst.

the two acidic sites ($Si^{+4}$ and $Fe^{+3}$ ions) are for the adsorption of two terminal OH groups of alkanediols, which is just as we proposed the adsorption structure for 1,4-BDO on ARB clay catalyst surface [16]. From this study, we also speculate that synchronous adsorption of alkanediols on ARB clay surface played a major role in the selective formation of THP and oxepane products scenario was shown in Figs. 14 and 15.

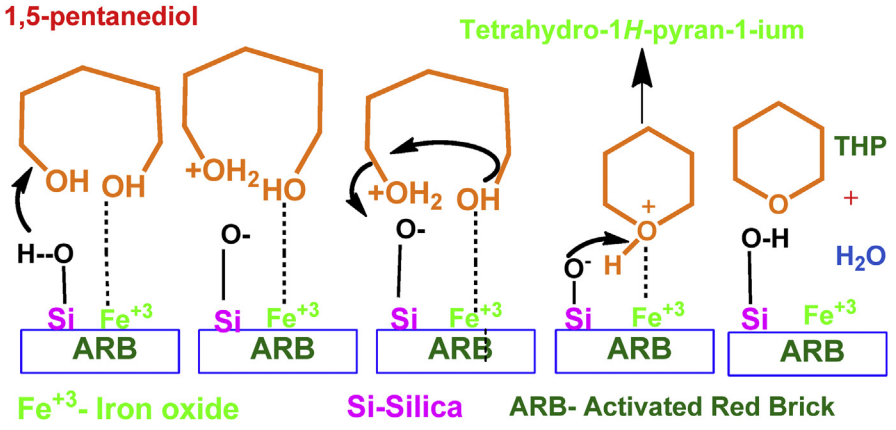


**Fig. 14.** A plausible reaction mechanism for 1,5-PDO dehydration on ARB clay catalyst.


https://doi.org/10.1016/j.heliyon.2019.e01212

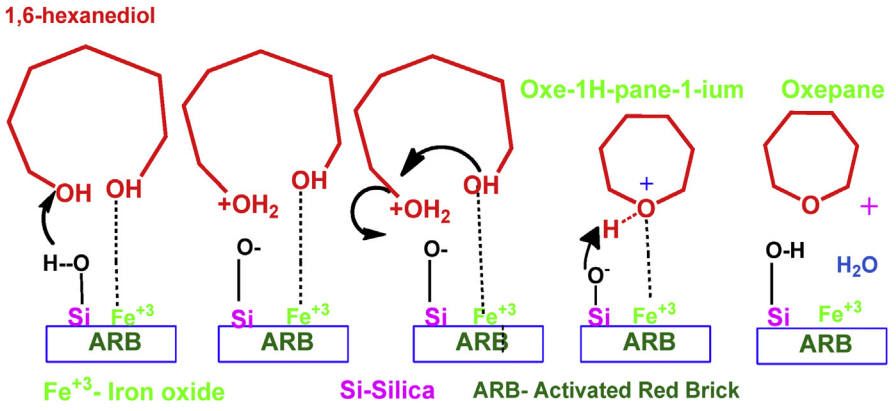


**Fig. 15.** A plausible reaction mechanism for 1,6-HDO dehydration on ARB clay catalyst.

In addition, weak to mild acidic sites generated on the surface of ARB clay catalyst vital influence in cyclised product distribution from 1,5, and 1,6-alkenediols rather than formation of dehydrogenation, Hoffman elimination products, hydrogenolysis products and other cyclised compounds.

In contrast, commercial silica and α-$Fe_2O_3$ catalysts showed noteworthy linear unsaturated 4-pentene-1-ol, 5H1OL selectivity as well as other cyclised products selectivity (shown in Tables 2 and 3). Figs. 10 and 11 illustrate the selectivity of THP and oxepane respectively using ARB and other commercial catalysts. Based on useful products (THP and oxepane) contribution, balanced $Si^{4+}$ and $Fe^{+3}$ ions in the ARB clay catalyst played a dramatic role in improved surface adsorption of 1,6-HDO and 1,5-PDO, which leads to maximum conversion.

## 5. Conclusions

In summary, selective vapour-phase dehydration of 1,5-PDO and 1,6-HDO was investigated over ARB clay catalyst, in comparison to commercial silica and α-$Fe_2O_3$ catalysts. The formation of THP from 1,5-PDO and oxepane from 1,6-HDO was efficiently enhanced by the Lewis and Bronsted acidic sites in ARB clay catalyst. Excellent selectivity of 82% THP and 89% oxepane with 100% conversion of respective substrates was achieved over ARB clay at 375 °C and 425 °C respectively. ARB clay catalyst showed sustained catalytic properties with sustained product selectivity throughout the time-on-stream activity. $NH_3$-TPD revealed that synergistic or combinational silica, iron oxide possessed ARB clay catalyst generated advantageous weak to mild acidic sites for superior THP and oxepane yields from 1,5-PDO and 1,6-HDO. Beyond the optimal temperatures of 375 °C and 425 °C, the dehydration of 1,5-PDO and 1,6-HDO showed mild THP and oxepane products selectivity due to facile transformations into other products contribution. Py-FT-IR acidic adsorption study reveals that better Lewis base interaction of 1,5-PDO, and 1,6-HDO with Lewis and Bronsted ARB clay catalyst.


https://doi.org/10.1016/j.heliyon.2019.e01212

## Declarations

### Author contribution statement

Venkata Rao Madduluri: Performed the experiments; Wrote the paper.

Naresh Kumar Katari: Analyzed and interpreted the data; Contributed reagents, materials, analysis tools or data; Wrote the paper.

Nagaiah Peddinti: Performed the experiments.

Challa Prathap: Performed the experiments; Analyzed and interpreted the data.

David Raju Burri, Seetha Rama Rao Kamaraju: Conceived and designed the experiments; Contributed reagents, materials, analysis tools or data.

Sreekantha B. Jonnalagadda: Analyzed and interpreted the data; Wrote the paper.

### Funding statement

This research did not receive any specific grant from funding agencies in the public, commercial, or not-for-profit sectors.

### Competing interest statement

The authors declare no conflict of interest.

### Additional information

No additional information is available for this paper.

### Acknowledgements

The author MVR grateful thanks to the University Grants Commission and Council of Scientific and Industrial Research, New Delhi, India for the award of fellow.

## References

[1] F. Zhang, B. Zhang, X. Wang, L. Huang, D. Ji, S. Du, L. Ma, S. Lin, Synthesis of tetrahydropyran from tetrahydrofurfuryl alcohol over Cu−Zno/$Al_2O_3$ under a gaseous-phase condition, Catalysts 8 (2018) 105−116.

[2] S. Basu, B. Ellingerr, S. Rizzoo, C. Deraevee, M. Schürmannn, H. Preutt, H.D. Arndtt, H. Waldmannn, Biology-oriented synthesis of a natural-product inspired oxepane collection yields a small-molecule activator of the Wnt-pathway, Proc. Natl. Acad. Sci. U. S. A. 108 (17) (2011) 6805−6810.


https://doi.org/10.1016/j.heliyon.2019.e01212

[3] Y. Brunel, G. Rousseau, Preparation of oxepanes, oxepenes, and oxocanes by iodoetherification using Bis(sym-collidine)iodine(I) hexafluorophosphate as electrophile, J. Org. Chem. 61 (1996) 5793−5800.

[4] Y. Inoue, S. Deguchi, T. Hakushi, Convenient one-step preparation of oxacyclanes by dehydration of diols over alumina, Bull. Chem. Soc. Jpn. 53 (1980) 3031−3032.

[5] S.E. Hunter, C.E. Ehrenberger, P.E. Savage, Kinetics and mechanism of tetrahydrofuran synthesis via 1, 4-butanediol dehydration in high-temperature water, J. Org. Chem. 71 (2006) 6229−6239.

[6] F. Sato, S. Sato, Dehydration of 1, 5-pentanediol over bixbyite Sc2-xYbxO3 catalysts, Catal. Commun. 27 (2012) 129−133.

[7] S. Sato, R. Takahashi, N. Yamamoto, E. Kaneko, H. Inoue, Vapor-phase dehydration of 1, 5-pentanediol into 4-penten-1-ol, Appl. Catal. A Gen. 334 (2008) 84−91.

[8] M.K. Gnanamani, G. Jacobs, M. Martinelli, W.D. Shafer, S.D. Hopps, G.A. Thomas, B.H. Davis, Dehydration of 1, 5-pentanediol over Na-doped $CeO_2$ catalysts, ChemCatChem 10 (2018) 1148−1154.

[9] S. Sato, F. Sato, H. Gotoh, Y. Yamada, Selective dehydration of alkanediols into unsaturated alcohols over rare earth oxide catalysts, ACS Catal. 3 (2013) 721−734.

[10] F. Sato, H. Okazaki, S. Sato, Dehydration of 1, 5-pentanediol over rare earth oxides, Appl. Catal. A Gen. 419−420 (2012) 41−48.

[11] H. Duan, M. Unno, Y. Yamada, S. Sato, Adsorptive interaction between 1, 5-pentanediol and MgO-modified $ZrO_2$ catalyst in the vapor-phase dehydration to produce 4-penten-1-ol, Appl. Catal. A Gen. 546 (2017) 96−102.

[12] M.K. Gnanamani, G. Jacobs, W.D. Shafer, S.D. Hopps, B.H. Davis, Dehydration of pentanediol over $CeO_2$, $CeO_2$-$Ga_2O_3$, and $CeO_2$-$In_2O_3$, Chem. Select. 2 (2017) 4150−4156.

[13] T. Akashi, S. Sato, R. Takahashi, Sodesawa, K. Inui, Catalytic vapor-phase cyclization of 1, 6-hexanediol into cyclopentanone, Catal. Commun. 4 (2003) 411−416.

[14] H. Grabowska, R. Klimkiewicz, J. Wrzyszcz, L. Syper, Catalytic reactions of pentamethylene and hexamethylene glycols over an iron oxide, J. Mol. Catal. A Chem. 154 (2000) 225−228.


https://doi.org/10.1016/j.heliyon.2019.e01212

[15] Y. Jyothi, P.V. Somaiah, K.H.P. Reddy, V. Venkateswarlu, K.K. Swamy, B. David Raju, K.S. Rama Rao, An inexpensive and environmentally friendly activated marble waste as a catalyst for vapour phase dehydration of 1, 4-butanediol to tetrahydrofuran, Catal. Commun. 101 (2017) 66–70.

[16] M. Venkata Rao, N. Chinna Krishna Prasad, K. Naresh Kumar, G. Venkata Siva Prasad, K. Thirupataiah, K. Seetha Rama Rao, Vapor phase selective tetrahydrofuran production from dehydration of biomass derived 1, 4-butanediol using ecofriendly red brick catalyst, Catal. Commun. 110 (2018) 38–41.

[17] G. Cultronea, I. Sidrabab, E. Sebastiana, Mineralogical and physical characterization of the bricks used in the construction of the "Triangul Bastion", Riga (Latvia), Appl. Clay Sci. 28 (2005) 297–308.

[18] U. Rafique, K.D. Biplob, Y.A.M. Mohammad, Synthesis and characterization of silica coated iron-oxide composites of different ratios, Int. J. Comp. Mater. 4 (2014) 135–145.

[19] S. Naga, A. Roychowdhury, D. Das, S. Mukherjee, Synthesis of α-$Fe_2O_3$-functionalised graphene oxide nanocomposite by a facile low temperature method and study of its magnetic and hyperfine properties, Mater. Res. Bull. 74 (2016) 109–116.

[20] E.A. Nadia El-Gamela, W. Laura, A. Karim, M. Sanjay, $SiO_2$@ $Fe_2O_3$ core–shell nanoparticles for covalent immobilization and release of sparfloxacin drug, Chem. Commun. 47 (2011) 10076–10078.

[21] W. Huixiong, Z. Mei, Q. Yixin, L. Haixia, Y. Hengbo, Preparation and characterization of tungsten-substituted molybdophosphoric acids and catalytic cyclodehydration of 1, 4-butanediol to tetrahydrofuran, Chin. J. Chem. Eng. 17 (2009) 200–206.

[22] G.M. Michael, G. Dinesh, S. Basudeb, K.P. Astam, B. Asim, M.M. Abu-Omar, Efficient solid acid catalyst containing Lewis and Brønsted acid sites for the production of furfurals, ChemSusChem 1–10 (2014) 2342–2350.

[23] B. Fouad, Y. Boucheffa, P. Ayrault, S. Mignard, P. Magnoux, NH3-TPD and FTIR spectroscopy of pyridine adsorption studies for characterization of Ag- and Cu-exchanged X zeolites, Microporous Mesoporous Mater. 111 (2008) 80–88.

[24] M.B. Nicolás, R.A. Carlos, J.M. Alberto, Liquid-phase dehydration of 1-phenylethanol over mordenite-like zeolites: influence of Si/Al ratio, Catal. Commun. 10 (2008) 261–265.


https://doi.org/10.1016/j.heliyon.2019.e01212

[25] B. Shuxing, D. Qiguang, C. Xinxin, W. Xingyi, Dehydrochlorination of 1, 2-dichloroethane over ba-modified al 2 o 3 catalysts, RSC Adv. 6 (2016) 52564−52574.

[26] C. Martin, P. Malet, G. Solana, V. Rives, Structural analysis of silica-supported tungstates, J. Phys. Chem. B 102 (1998) 2759−2768.

[27] I.B. Tazul, A. Palani, N.A. Muhammad, M.A. Abdullah, H.A. Raed, M. Al-Yami, Sulaiman, S. Al-Khattaf, Metathesis of 2-butene to propylene over W-mesoporous molecular sieves: a comparative study between tungsten containing MCM-41 and SBA-15, Appl. Catal. A Gen. 467 (2013) 224−234.

[28] L. Ying, F. Zhaochi, L. Yuxiang, S. Keqiang, Z. Lei, J. Guoqing, Y. Qihua, L. Can, Direct synthesis of highly ordered Fe-SBA-15 mesoporous materials under weak acidic conditions, Microporous Mesoporous Mater. 84 (2005) 41−49.

[29] V. Mohan, C.V. Pramod, M. Suresh, K. Hari Prasad Reddy, B. David Raju, K.S. Rama Rao, Advantage of Ni/SBA-15 catalyst over Ni/MgO catalyst in terms of catalyst stability due to release of water during nitrobenzene hydrogenation to aniline, Catal. Commun. 18 (2012) 89−92. Contents lists available at SciVerse.

 https://doi.org/10.1016/j.heliyon.2019.e01212